Structural, Opto-electronic, and Photocatalytic Properties of some pure and Al/Ni modified ZnO

M.Sc. Thesis

By

Kailash Dukiya

Department of Physics
Indian Institute of Technology Indore
June 2022

Structural, Opto-electronic, and Photocatalytic Properties of some pure and Al/Ni modified ZnO

A Thesis

Submitted in partial fulfillment of the
requirements for the award of the degree

of

Master of Science

By

Kailash Dukiya

Department of Physics
Indian Institute of Technology Indore
June 2022

Indian Institute of Technology Indore

Candidate's Declaration

I hereby certify that the work which is being presented in the thesis entitled **Structural, Opto-electronic, and Photocatalytic Properties of some pure and Al/Ni modified ZnO** in the partial fulfillment of the requirements for the award of the degree of **Master of Science** and submitted in the **Department of Physics, Indian Institute of Technology Indore**, is an authentic record of my work carried out during the time period from July 2021 to June 2022 under the supervision of **Dr. Somaditya Sen, Associate professor, Indian Institute of Technology Indore.**

The matter presented in the thesis has not been submitted by me for the award of any other degree at this or any institute.

Kailash

06/06/22

Signature of student with date

(Kailash Dukiya)

This is to certify that the above statement made by the candidate is correct to the best of my knowledge.

Somaditya

Signature of the Supervisor of
M.Sc. thesis (with date)
(**Dr. Somaditya Sen**)

Kailash Dukiya has successfully given his M.Sc. thesis.

Somaditya

Signature of supervisor of MSc thesis
(Dr. Somaditya Sen)
Date: 6/6/22

Signature of convener, DPGC
Date: 6/6/2022

Signature of PSPC member
(Prof. Rajesh Kumar)
Date: 6/6/2022

Signature of PSPC member
(Prof. Krushna R. Mavani)
Date: 06/062022

Abstract

$\mathrm{Zn_{1-x}(Al_{0.5}Ni_{0.5})_x\,O}(\mathrm{x} = 0, 0.0078, 0.0156, 0.0234, 0.03125)$ nanoparticles have been synthesized by using a simple sol-gel route. ZnO generally crystallizes in three forms: hexagonal wurtzite, cubic Zinc Blende and rock salt structure. According to the first principle, periodic Hartree-Flock linear combination of atomic orbitals theory, the hexagonal Zinc wurtzite is found to be the most thermodynamically stable form.

It was observed from XRD studies. A Rietveld analysis of the XRD spectra using GSAS software helped evaluate the variations of lattice constant, lattice strain, lattice parameter around a = b = 3.25 Å, c = 5.20 Å of pure ZnO and doped one. With Al/Ni doping, while the direct bandgap could be nominally tuned from ~ 3.247 eV to ~ 3.273 eV, the Al/Ni doping seems to improve carrier concentration, mobility, and lattice regularity than pure ZnO. The photocatalytic degradation of toxic methylene blue (MB) dye could be enhanced from $0.560 \leq x \leq 3.125\%$ Al/Ni doped ZnO. This property has been correlated to the carrier properties of the materials. This n-type is due to the structural point defect (vacancies and interstitials) and extended defects (threading/planar dislocations).

Acknowledgements

First and foremost, I'd like to express my gratitude to Dr. Somaditya Sen, my supervisor, without whose direction and unwavering support it would have been difficult for me to have a deeper understanding of the subject. Working under his for my thesis has been a tremendous honor, and it goes without saying how much his knowledge, supervision, and support have aided my development, not only academically but also personally. He, as a mentor, provided essential advice and bolstered my spirits anytime I encountered adversity, and I will be eternally grateful.

I am thankful to Prof. Krushna Mavani & Prof. Rajesh Kumar for being my PSPC committee members. I am immensely thankful to the entire faculty of the Department of Physics at IIT Indore for all the courses which I have been taught during my degree and for conducting my seminar in such a smooth and efficient manner.

I am extremely thankful to all of my lab seniors for their encouragement and invaluable assistance. I am thankful to Mr. Suresh Baral (Buddy) and Maneesha ma'am (PMRF) for guiding me. I am also thankful to Mukul sir and Koyal ma'am (PMRF).

I want to express my gratitude to my parents for allowing me to pursue my dreams and objectives while also guiding me in every part of my life.

I would like to offer my special thanks to Diksha Sharma for her assistance in my thesis and also for supporting me in my hard time. Her true believe in me gives confidence and strength. My thanks and appreciations also go to my colleagues in developing the project and to the people who have willingly helped me out with their abilities. You can't thank people for the love and care they provide to you. Their love and support makes me a better man. They all gonna be in my heart forever. Special thanks to members of 304 group, especially Amarendra, Satya, Ramavtar, Ankush, Bhavin, Ankur and Sayak. This thesis is a dedication to all I've learned about life through my family, friends, instructors, and supervisors, as well as a tribute to the enormous amount of effort I've put into it.

Contents

List of Figures

Chapter 1

Introduction and Importance of ZnO

A simple oxide is one carrying some oxygen atoms that the normal valency of its metal allows. Examples- ZnO, CuO, NiO, MgO, and Al_2O_3 . We get a mixed oxide upon the combination of two simple oxides. Many types of oxides are classified based on their chemical behavior e.g.- Acidic oxides, Basic oxides, and Amphoteric oxides. The process of sample preparation, characterization of sample, and application basis on the characterization of mixed oxides in recent years has received increasing interest because of the many physical and optoelectronic properties of these metal oxides. Nanomaterials have attracted several researchers from different fields due to their unique properties and potential applications in different areas such as spintronics devices, transparent electronics, piezoelectricity, optoelectronics, etc.

1.1 Zinc Oxide (ZnO)

Zinc oxide is a type of inorganic compound. The chemical formula is ZnO. ZnO is a white powder that is insoluble in water. ZnO is used as an additive in numerous materials and products including, rubbers, plastics, ceramics, glass, cement, etc.
ZnO can be shaped like a rod, star and the size may lie between 30-50 nm. The defected active oxygen species generated by these metal oxide ZnO are used in applications like many cosmetics items and personal care products including mineral makeup, nail products, bath soaps, and face powders. It is also good in water wash UV protection.
ZnO is a very active material in different applications such as optoelectronics, spintronics, piezo electronic catalysts, solar cells, UV absorbers, and photoelectric devices. ZnO has a large direct bandgap in the range of 3.1 to 3.3 eV and for bulk

material large exciton binding energy approximate (60 meV) are very good for electronic properties. We know ZnO is a type of semiconductor due to intrinsic defects. There are some more interesting properties like green synthesis properties of ZnO, and also bio study. The correlation of structural change can be observed by using X-ray diffraction also gives the knowledge of bond length, bond angle, and the detailed information about chemical structure phase a polymorphology. The modification in band properties was observed experimentally and theoretically. The band gap energy observed in UV range

1.1.1 Crystal Structure

ZnO generally crystallizes in three forms: Hexagonal Wurtzite, Cubic Zinc Blende, and Rock salt structure. According to the first principle of periodic Hartree-Fock linear combination of atomic orbitals theory, the hexagonal Zinc wurtzite is found to be the most thermodynamically stable form [1]. It belongs to the space group of P63mc [1,2] which has two lattice parameters; a= 3.25 Å, c= 5.20 Å and is characterized by two interconnecting sub lattices of Zn^{2+} and O^{2-} where each anion is surrounded by four cations at the corners of a tetrahedron with a typical sp^3 covalent bonding. The number of alternating planes of tetrahedrally coordinated O^{2-} and Zn^{2+} ions which are pilled alternately along the c-axis (Figure 1.1) describe the Wurtzite structure of ZnO. The zinc and oxide center in the wurtzite ZnO is tetrahedral and this tetrahedral symmetry plays an important role in the polarity of ZnO. Piezoelectricity and pyroelectricity are the direct consequences of the polar symmetry of ZnO along the hexagonal axis. ZnO is generally found to be an n-type structure. This n-type structure is due to the structural point defect (vacancies and interstitials) and extended defects (threading/planar dislocations). The presence of oxygen vacancies in the ZnO lattice gives it n-type conductivity.

1. Physical properties: Pure ZnO is white and turns yellow on heating. Its molecular weight is 81.37 g/mol. ZnO has a relative density of 5.607 . Under high pressure, the melting point of ZnO is 1900^{o}C and its heat capacity is 9.62 Cal/deg/mole at 25^{o}C. It is insoluble in water but soluble in acid. During the application of pressure, the lattice becomes compact. At melting temperature, there is a volumetric expansion in the lattice. Applying pressure suppresses the volumetric expansion and therefore delays the melting point.

2. Opto-electronic Properties: ZnO has a large exciton binding energy around 60 meV at room temperature due to excitonic recombination [3]. This large

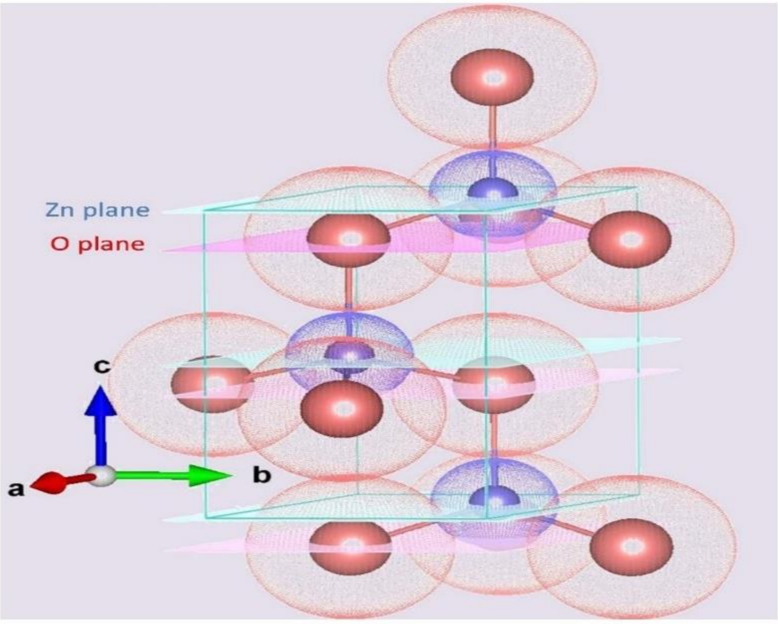

Figure 1.1: Crystal structure of ZnO (Tetragonal lattice)

exciton binding energy makes efficient excitonic emission in ZnO suggests that ZnO is a promising material for optical devices at room temperature or higher. The process of optical absorption and emission are very much influenced by transition related to dopants or defects which are usually responsible for creating a mid-gap discrete electronic state [3]. Many reports show that the photoluminescence of ZnO shows green emission and the intensity of green emission increases with decreased particle size and reduced nanowire diameter which gives a quantum size effect. The reduction in particle size increases the binding energy which in turn enhances the optoelectronic property of ZnO nanomaterial.

3. Optical Properties: As reported in different literature, the optical band gap of ZnO is 3.44 eV at low temperature (4 K) and 3.3 eV at room temperature [4] which corresponds to the energy of 375.75 Å photons. So, zinc oxide is transparent to visible light but strongly absorbs ultraviolet light below 375.75 Å. Due to this reason, ZnO is used in varieties of optoelectronic applications like Light Emitting Diode (LEDs), Solar Cells, photodetectors, etc. [1,5–7]. The band gap of ZnO depends upon the carrier concentration. The band gap tends to decrease as there is an increase in carrier concentration. Photoluminescence of ZnO represents a relatively sharp absorption peak at 380nm (due to band-to-band transitions) and a wider yellow-green emission band (due to the presence of oxygen vacancies and other related defects.
   ZnO has a wide bandgap of 3.3 eV at room temperature. This wide band gap

has many advantages like higher breakdown voltage, ability to sustain large electrical fields, lower electronic noise, high temperature, and high- power operation. These properties make ZnO nanomaterial fit for a wide variety of electrical applications. The electron mobility of ZnO strongly depends on temperature and possess a maximum of $\sim$2000 cm^2 / (V·s) at 80 K.

4. Mechanical Properties: ZnO is a relatively soft material with approximate hardness $\sim$ 5. Its elastic constants are smaller than other materials belonging to the same group. The high heat conductivity, low thermal expansion, and high melting temperature of ZnO are some of the basic characteristics of ZnO nanomaterials. High thermal conductivity makes it useful in the rubber industry. ZnO is added to the rubber to increase the thermal conductivity. ZnO exhibits high radiation hardness property which makes it useful in space or at high altitudes [7,9].

5. Magnetic Properties: Various reports show that room temperature magnetism can be achieved by doping magnetic impurity in ZnO like Fe, Pb, Co, etc. But preserving magnetism at room temperature in this material is still a challenge. Despite many experimental results, the reason behind the origin of magnetism in this material is not clear. In some cases, it is explained in terms of the segregation of metallic clusters [10] while in other cases it is due to double exchange [11,12]. Double exchange occurs between ions of different oxidation states which predicts the way by which electrons are transferred between two species.

1.1.2 Zinc Oxide Nanoparticles

Zinc oxide nanopowder is among one of the most researched studies conducted due to its ability to apply in varied downstream applications. Zinc oxide is inexpensive, safe, and as well as it can be prepared easily by several methods. The physical and chemical behaviors of zinc oxide nanopowder can be easily tuned by changing the morphology by using different synthesis techniques or different precursors or different materials to produce the nanomaterial.

Zinc oxide nanoparticle is one of the inorganic compounds of group II-IV semiconductor for analytical sensing applications. Zinc oxide nanoparticle appears to be white powder and insoluble in water. Zinc oxide nanoparticle has an energy band of 3.37 eV and bonding energy of 60 meV, which provides excellent chemical, electrical, and thermal stabilities. Zinc oxide nanoparticle also has optical, electrical, and photocatalytic properties.

Due to these properties, zinc oxide nanoparticle is applied in solar cells, photocatalysis, and chemical sensor. Zinc oxide nanoparticle is also known for their low toxicity and high UV absorption, making it a good candidate to be used in the biomedical field. Zinc oxide nanoparticle also has a hard and rigid structure making it useful in the ceramic industry.

One of the advantages of using zinc oxide nanoparticles in the biomedical field is that they act as a good surface material. Zinc oxide nanoparticle is naturally known for their strong resistance to microbes. Due to these reasons, zinc oxide nanoparticle is extensively used for biological labeling, biological sensing, drug delivery, gene delivery, and nanomedicine. Food and drug administration has approved zinc oxide as a safe material. Zinc oxide also can solubilize in an acidic environment therefore, this allows the material to be discovered as multifunctional nanocarriers to ease the drug-delivering and release processes.

The bandgap of the material is changed because of the discretization of the electron energy, which can be controlled by the nanometer size particles. Such quantum dots behave like atoms and become luminescent. Their emission can be continuously tuned through a large spectrum by changing their size. On decreasing the size, the electron gets confined to the particle (confinement effects) leading to an increase in bandgap energy and band levels get quantized (discrete). By reducing size of the particle, the density of states become more quantized and the bandgap shifts to higher energies (shorter wavelengths). By changing the size of the nanoparticles, the frequency of emission can be tailored. ZnO nanostructures are one of the intense interest as they can be prepared by a variety of methods and in a range of different morphologies like nanorods, nanobelts, nanoflowers, nanoneedles, nanorings, etc. The Vapour phase synthesis method is the most extensively and commonly used method by the different research groups for the synthesis of 1-D nanorods or nanowires. The typical vapour phase synthesis method includes vapour liquid-solid (VLS) growth, chemical vapor deposition (CVD), metal-organic chemical vapour deposition (MOCVD), physical vapor deposition (PVD), molecular beam epitaxy (MBE), pulsed laser deposition (PLD), metal organic vapour phase epitaxy (MOVPE). Nano flower and nano belts are mainly synthesized by using hydrothermal, solid-state process, pyrolysis, wet chemical method, precipitation process, and many other methods. However, the primary motive of ZnO research is its great potential for a variety of practical applications, such as in optoelectronic devices, energy harvesting devices, electronic devices, sensors, catalysts, active compounds in sunscreens, etc.

Chapter 2

Experimental and Theoretical Methodology

This chapter provides basic initial information about the synthesis procedure (sample preparation) and characterization techniques used in research work. All presently studied samples have been prepared using sol- gel synthesis prosses. As far as characterization techniques are concerned, we have performed:

1. X-ray diffraction (XRD) to confirm the formation of the structural phase.
2. FESEM to study morphology and size of the material.
3. EDS to confirm the chemical composition of the material.
4. Raman spectroscopy to study the changes in vibrational modes in pure and doped ZnO (v) UV-Vis spectroscopy to study the band gap tailoring affected by the defect states generated by doping.
5. Photoluminescence spectroscopy to study the defect states and related optical properties (color emission) of the materials. It has been used for the analysis of structural and physical properties.

Further, more specific details about the synthesis of samples and characterization techniques are discussed accordingly in the 'experimental' section of this chapter. The functionalities of these materials were looked into in the domains of humidity/light sensing and their utilization capabilities as transparent conductive oxides and UV sensors.

The synthesis and characterization for $Zn_{1-x}(Al_{0.5}Ni_{0.5})_xO$ (x=0, 0.0078, 0.0156, 0.0234, 0.03125) are briefly discussed in this chapter.

A modified sol-gel process is used to synthesize the samples, which is then followed by successive high-temperature annealing. The following characterization techniques were used to investigate material properties: x- ray diffraction to confirm phase purity and crystal structure, Raman spectroscopy to study vibrational properties, and UV-Visible spectroscopy to calculate bandgap energy and Urbach energy.

2.1 sol-gel method

The sol-gel method is one of the most well-establish and simple methods for the preparation of nanoparticles. From this method we can prepare sample on large scale. This method has potential control of the whole reaction during synthesis. Generally in this method, we use nitrides, and chlorides to form oxides.
Chemical precursors citric acid and ethylene glycol vigorously mixed for an hour. They react to form monomers and later form polymers upon heating the polymeric solution works as gelling agent. When we heat it at high temperature the polymeric chain break and releasing energy, thereby a burning agent the gelling solution was added to the homogenously mixed precursor solution. Mild heaty (∼50 c) ensures homogenous attachment of the homogenously to polymeric chain.
The transparency of the solution was maintained by contrary the alkalinity or acidity of solution. The gel formed after dehydration of the solution the dehydration process continued until the gel dried out to give burnt ashes. These burnt ashes contain precursor ions and some remnants of the polymers in the form of C and N polymers. Compounds Denitrification of the dried gel ashes was done by heating at 450°C for 6hrs. Samples were the after heat at 600°C for at decarbonization.

2.2 Synthesis Process

2.2.1 Preparation of Pure Sample

ZnO nanoparticles were synthesized by sol-gel method [9] (standard Pechini method) followed by solid state sintering. Schematic diagram and experimental steps evolved in nano powder synthesis using sol-gel technique is shown in Figure 2.1. ZnO powder (Alfa Aesar, purity 99.9%) was dissolved in HNO_3 [$ZnO + 2HNO_3 \uparrow Zn(NO_3)_2 + H_2O$] to form a Zn solution.
A polymeric solution was formed by concentrated glycerol (Alfa Aesar, 99.9%) in deionized water at 70°C for 4 hrs. The Zn solution was then added to the polymeric solution. This solution was stirred and heated on hot plates at ∼60°C to obtain finally "gel-ready solution". The Zn ions get attached homogenously to the chains of the polymeric solution. The solution was gradually dehydrated to form gel in ∼4hrs.

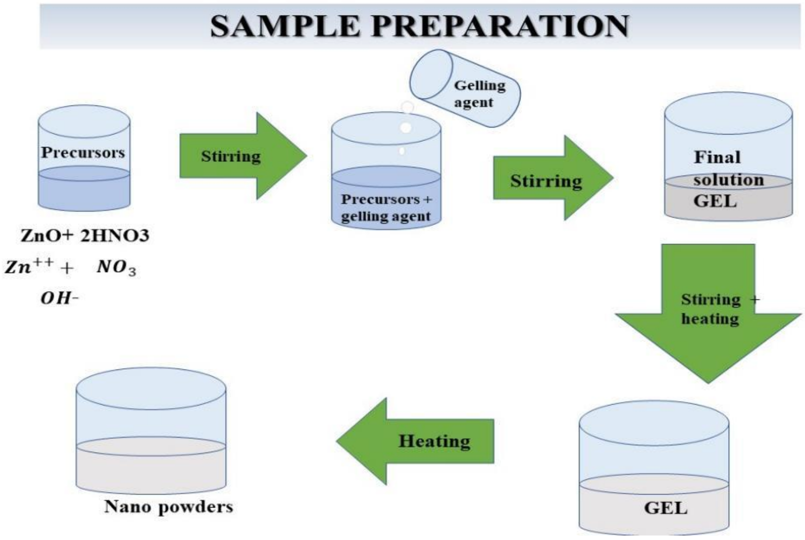

Figure 2.1: Steps involved in Sol-Gel process

$Zn(NO_3)_2 + C_6H_8O_7 + C_3H_8O_3(C_2H_5 - O - Zn - O - C_2H_5)_n \uparrow ZnO + H_2O + N_2$ $+CO_2$. The gel was burnt on hot plates in ambient conditions to obtain yellowish white colored powders. These resultant powders were decarbonized and denitrified by heating in air at 450°C for 6 hrs to form white powders of ZnO. The powders were further annealed at 600°C for 2 hrs. For electrical characterization, the obtained white powders were pelletized under 4T pressure and sintered at 600°C for 2 hrs.

2.2.2 Doped Sample Preparation

For all doped samples the final “gel-ready solutions” were prepared by obtaining a mixed solution of the constituent elements in the right proportion. For all the doped samples the gels were burnt, decarbonized and denitrified similar to the process discussed in section 2.1.
Annealing temperature and time were chosen by considering solubility limit of dopant. In case of Si and Si/Na doped ZnO, annealing temperature chosen was 600°C since beyond it, s samples since at a lower growth time, the formation of small particle is kinematically favored. The formation of small particles reduces the super saturation and hence the possibility of coalescencing/agglomerating. The processes of obtaining these solutions are discussed in the following sections.

Al^{3+}/Ni^{2+} doped ZnO synthesis

$Zn_{1-x}(Al_{0.5}Ni_{0.5})_x$ were synthesized for x = 0, 0.0078, 0.0156, 0.0234 and 0.03125 and named Z(AN)S0, Z(AN)S1, Z(AN)S2 Z(AN)S3and Z(AN)S4 respectively.
Aluminum nitrate (molar mass 212.997 g/mol) [$Al(NO_3)_3.9H_2O$] and nickel ni-

trate (molar mass 182.703 g/mol) [$Ni(NO_3)_3.6H_2O$] were used as a precursor for Al^{3+}/Ni^{2+} respectively . Appropriate amount of Al and Ni precursor was dissolved in distilled deionized water (DDIW). These Al and Ni solutions were then added to appropriate amount of Zn solution (prepared similarly as Section 2.1) to achieve Z(AN)S0, Z(AN)S1, Z(AN)S2 Z(AN)S4and Z(AN)S5. The obtained homogenous mixtures containing Zn and Al, Ni and Zn ons were rigorously stirred for several hours to obtain the "gel-ready solution".

ZnO generally crystallizes in three forms: hexagonal wurtzite, cubic zinc blende and rock salt structure. According to the first principle periodic Hartree-Fock linear combination of atomic orbital theory, the hexagonal zinc oxide wurtzite is found to be the most thermodynamically stable form [16]. Structural parameters like lattice parameters, strain, size etc. plays an important role in determining its bandgap and other optical properties. Lattice parameters mainly depend upon the following factors [17]:

1. Free electron concentration occupying conduction band minima.
2. Concentration of foreign substituted/doped atoms.
3. Defects in lattice
4. Difference in ionic radii of host and substituted atom.
5. Strain
6. Temperature

Depending upon the properties of the aliovalent ion, i.e., charge, size and electronic properties, local structural changes takes place. It is generally the case that a higher charged ion will be able to retain or hold more oxygen in the lattice while a lesser charged ion will retain less oxygen thereby creating oxygen deficiencies. However, as much as less oxygen may generate strain in the lattice, same may happen in case of excess oxygen. Much depends on the ionic radius of the dopant on how much oxygen can be retained or driven away from the lattice. Hence, aliovalent ion doping or substitution generally generates distortion in the lattice introducing strain and thereby defects in structural properties of pure and modified ZnO lattice [18]. At some amount of substitution, the lattice can no longer sustain the internal strain and reorganize overall structure of ZnO lattice. In this chapter, we have done detailed investigation of the effect of aliovalent ion doping in ZnO for samples Al^{3+}/Ni^{2+} on structural properties of ZnO. The changes in lattice parameters, strain, vibrational modes, size etc has been studied in detail.

Effect of Al^{3+}/Ni^{2+} Doping on Structural Properties of ZnO

Different concentrations of silicon were doped in ZnO lattice. When an Al^{3+} ion (crystal radius $\sim$ 0.54A) is doped in ZnO lattice, Si may go to an interstitial position due to its small size compared to both Zn^{2+} and O^{2-} ions (crystal radius $\sim$ 0.74Å and 1.24Å respectively [19]). However, due to its +3 charge, Al^{3+} will locally draw more oxygen than Zn^{2+}. To compensate charge, a tendency of reduction of positive charge is natural. Thus, incorporation of Al^{3+} will decrease oxygen vacancy VO. Hence, logically a substitution scenario is more probable, where lattice will arrange itself to accommodate Al^{3+} in the position of Zn, rather than an interstitial scenario. But this cannot continue for long as soon the VO type of defects will be taken care of by the excess oxygen dragged by increasing Al^{3+} concentration. The excess oxygen will drive the lattice to locally modify to other structures. However, all these changes must modify ZnO lattice parameters, strain, vibrational modes, electronic structure etc. There are limited number of reports present on Al doped ZnO [20,21–24]. Deep analysis of structure and opto- electronics properties of these systems needs to be done. The calcined samples were annealed at 600°C for 2 hrs.

2.3 X-ray Diffraction

X-Rays are generated in a cathode ray tube by heating a filament to produce electrons, accelerating the electrons toward a target by applying a voltage, and bombarding the target material with electrons. When electrons have sufficient energy to dislodge inner shell electrons of the target material, characteristic X-ray spectra are produced. These spectra consist of several components, the most common being Kα and Kβ . The specific wavelengths are characteristic of the target material (Cu, Fe, Mo, Cr). Copper is the most common target material for single-crystal diffraction, with Cu Kα radiation = 1.5418 Å. These X-rays are collimated and directed onto the sample. As the sample and detector are rotated, the intensity of the reflected X-rays is recorded. Cnstructive interference occurs and a peak in intensity occurs, when the geometry of the incident X-rays impinging the sample satisfies the Bragg Equation ($n\lambda = 2dSin\theta$) as shown in Figure 2.2.

X-ray diffraction is currently a widely used technique for investigating crystal structures and atomic spacing. A cathode ray tube generates the X-rays, which are then filtered to produce monochromatic radiation, concentrated by a collimator, and directed onto the sample. After that, the diffracted X-rays are detected, processed, and tallied. Due to the random orientation of the powdered material,

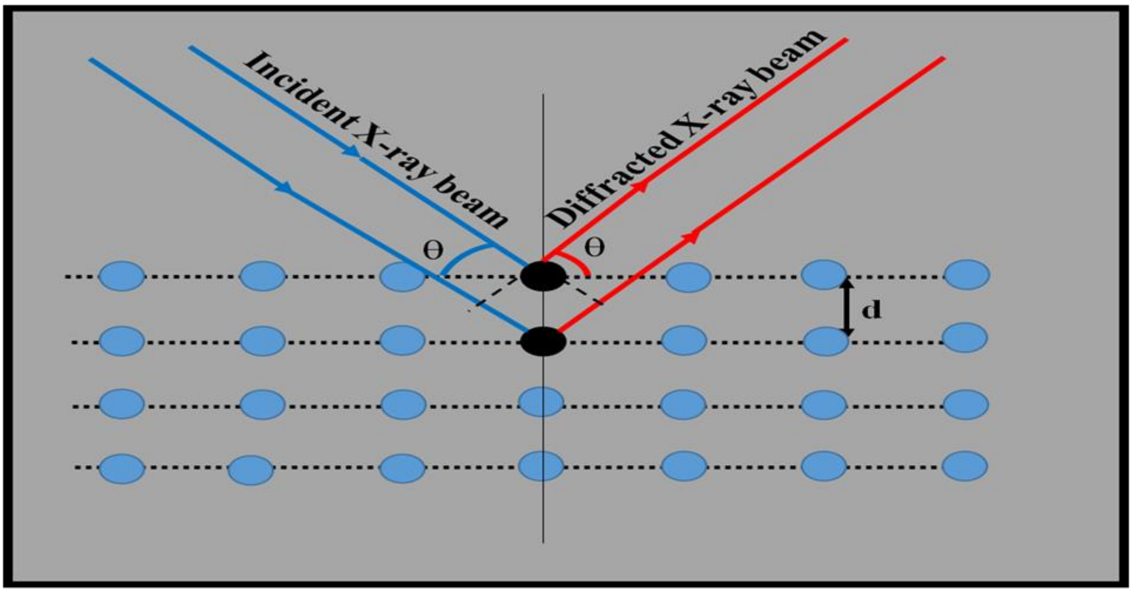

Figure 2.2: Bragg reflection in the atomic planes of crystal lattice

all potential diffraction directions of the lattice should be acquired by scanning the sample through a range of 2θ angles.
The essential components of a diffractometer are:

- X-ray Tube:- X-ray source: To condition the X-ray beam before it touches the material, use a direct beam slit.
- Soller slits govern the sideways divergence of either the incident or dispersed beam. The platform that holds and moves the sample, optics, detector, and/or tube is known as a goniometer.
- Sample Holder for samples Detector slits used to condition the X- ray beam after it has passed through the sample. The detector counts the number of X-rays scattered by the sample.

2.4 Field Emission Scanning Electron Microscope (FESEM)

Morphological study of specimen has been carried out using FESEM [13]. In this work, FESEM images were recorded using Supra T M 55; Carl Zeiss.

In FESEM, electrons are incident on the surface atoms, very similar to visible light falling on matter. Due to a much smaller size of electron as compared to visible light it can resolute much better and can thereby see the sample's surface, topography, morphology. The energized electrons sometime while interacting with

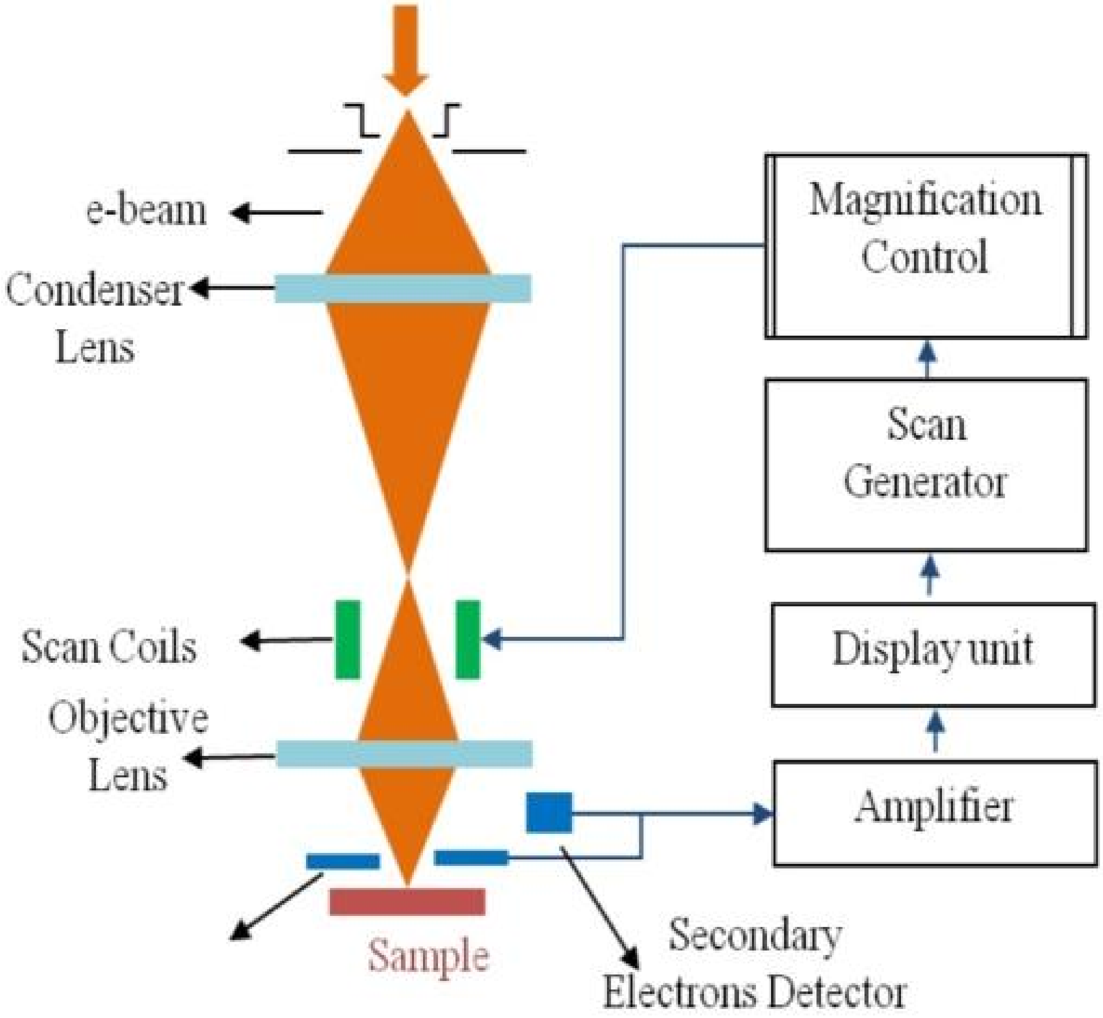

Figure 2.3: Schematic Diagram of FESEM instrument

the atoms are capable of knocking X-ray from the same, by analyzing the X-ray spectrum, and thereby the composition of the materials. The interaction of electron and matter results in emission of secondary electrons (SEs), backscattered electrons (BSEs), Auger electrons, X-rays, etc. A FESEM instrument uses SEs & BSEs for generation of images and X-rays for elemental analysis.

1. Secondary electrons: Secondary electrons originate from the surface or near-surface region of the samples as a result of inelastic interaction between primary electron beam and the samples. They have lower energies ($E < 50eV$) and therefore electrons are ejected within few nanometers of the sample surface. In this work, the ejected electrons are detected by Everhart- Thornley detector.

2. Backscattered electrons: Backscattered electrons originate from broad region within the interaction volume. They generate due to elastic interaction be-

tween electrons (from electron gun) and atoms in the specimen which results in a change in electron trajectory. Backscattered electrons consist of high-energy electrons (E $>$ 50eV), that are reflected by the specimen interaction volume by elastic scattering interactions with specimen atoms. Solid state detectors are used to detect backscattered electrons.

3. Imaging in SEM: When the primary electron beam interacts with the sample, the electrons lose energy by repeated scattering and absorption. This interaction volume extends from less than 100 nm to approximately 5 µm into the surface. The size of the interaction volume depends on the electron's energy, the atomic Experimental Details 43 number of the specimen and the specimen's density. The energy exchange between electron beam and sample results in the reflection of high-energy electrons by elastic scattering, emission of secondary electrons by inelastic scattering and the emission of electromagnetic radiation, each of which can be detected by specialized detectors. The beam current absorbed by the specimen can also be detected and used to create images of the distribution of specimen current.

2.4.1 Construction of Instrument

The SEM requires an electron probe, a specimen stage to place the specimen, a secondary-electron detector to collect secondary electrons, a solid-state detector to collect backscattered electrons, an image display unit, and an operation system to perform various operations.

(a) Electron source: The illumination system of FESEM consists of an electron source which is maintained at a negative potential. The emitted electron beam, which typically has an energy ranging from a 100 eV to 30 KeV is passed through a magnetic lens system.

(b) Condenser lens and objective lens: The electron beam is further focused by a condenser lens to a spot 0.4-5 nm in diameter. Two-stage lenses are located below the electron gun. The objective lens determines the final diameter of the electron probe up to 5 to 10 nm.

(c) Detector: A scintillator is coated on the tip of the detector and a high voltage of about 10 Kev is applied to it. The electrons hit the scintillator and generate light. Secondary electrons are detected by Everhart-Thornley detector. These electrons are accelerated towards a phosphor or scintillator positively biased to about +2,000 V. The accelerated secondary electrons are sufficiently energetic to emit flashes of light by the scintillator. A light pipe carries the photon signal from the scintillator inside the evacuated specimen chamber of the SEM to the photomultiplier outside the chamber. The amplified electrical signal output by the photomultiplier is displayed as a two-dimensional intensity distribution that can be viewed and photographed on an analogue video display, or subjected to analog-to- digital. The Everhart-Thornley detector is inefficient for the detection of backscattered electrons because it is positioned to one side of the specimen and also low positive charge cannot attract high energy electrons. Therefore, solid state detectors are normally used having a p-n junction. Electrons which escape the sample are absorbed by the detector and electron-hole pairs are generated. The number of these electron-hole pairs depends on the energy of backscattered electrons. One of the two electrodes of the p-n junction attract electrons while the other holes, thereby generating an electrical current. The value of the current is therefore proportional to number of backscattered electrons. The results are displayed on a liquid crystal display (LCD).

2.5 Raman Spectroscopy

Raman spectroscopy is a spectroscopic technique used to observe vibrational, rotational and other low frequency phonon modes in a system [14]. It relies on inelastic scattering (Raman scattering) of monochromatic light (usually from a laser in the visible, near infrared or near ultraviolet range). The experimental set-up of Raman spectroscopy is shown in Figure 2.4.

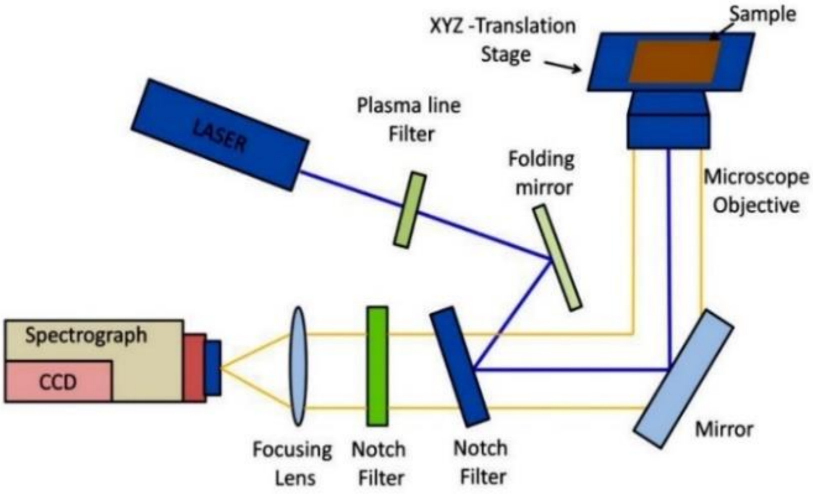

Figure 2.4: Experimental set-up of Raman spectroscopy

Laser light interacts with phonons i.e., molecular vibrations in the system, resulting in modification of light. The modification gives information about the energy of the phonons of the system. The reflected light from the illuminated spot is collected with a lens and sent through a monochromator. Most of the reflected light is elastically scattered and is of the same wavelength as of the incident laser line (Rayleigh scattering). This is filtered out by either a notch filter or a band pass filter. Rest of the collected light is dispersed onto a detector. Spontaneous Raman scattering is typically very weak. Separating the weak inelastic Raman scattered light from the intense Rayleigh scattered laser light is a criticality. In this work Raman measurement was carried out on a RIR-M151 Research India micro- Raman system at room temperature, using 532 nm line of diode laser as an excitation source with 75 mW power.

a) Laser: Diode laser (Research Spectra) was used as an excitation source for Raman scattering experiments. Laser emission was accompanied by many spurious spontaneous emission lines which must be eliminated to avoid interference with the Raman emissions. Therefore, a laser-filter monochromator with a band pass of 1.0 nm (and transmission of 75 %) was used to eliminate the undesired plasma lines.

b) Filter and microscope: Standard microscope with three plan achromatic objectives 10X, 50X and 100X, optically adapted to the aperture of the instrument. Other objectives with lower magnification can be used without a correct aperture adaptation which might introduce some vignetting effect. With the microscope, incident and scattered optical axis are identical i.e. back scattering geometry. Notch filters are used to remove Rayleigh scattering and pass Stokes and Anti-Stokes spectra. Normal mirrors and folding mirrors are used to focus the laser towards samples.

c) CCD detector and recording system: For this system, Peltier cooled CCD was used, working at 215K is selected to offer highest performance to the system. Spectrometer is controlled by Research India software. The computer-controlled scan range, integration time, scan speed and different scan units are available with the software.

2.6 UV-Vis Absorption Spectroscopy and Diffuse Reflectance Spectroscopy

When electromagnetic radiation (light) interacts with matter, various effects can be observed such as reflection, scattering, absorbance, transmittance and fluorescence/

phosphorescence. Total potential energy of a molecule can be represented as the sum of its electronic, rotational and vibrational energies. When energy of incident light is equal to the energy required to excite an electron from a lower energy level to higher level, the light is absorbed.

Working Principal: Amount of light absorbed is the difference between the incident radiation (I_0) and the reflected or transmitted radiation (I). Quantitatively absorbance is described by equation: A = -log(I/I_0). where, A is absorbance, T is transmittance, Io and I are the intensities of incident and transmitted light respectively at a given wavelength. A UV- Vis spectrophotometer uses a tungsten-halogen or deuterium lamp as a source. A dispersion device like a monochromator is used to select the incident wavelength. A detector, which converts UV-visible light into electrical signal is the final component of the spectrophotometer. It is easy to bandgap (E_g) from absorption spectra, in case of solid films of known low thickness, due to low scattering properties. However, in colloidal samples, due to large surface area exposure scattering is enhanced. As dispersed light does not reach the detector it is counted as absorbed light. The technique (optical absorption) cannot distinguish between the two phenomena.

UV-Vis of powdered sample is carried out by dispersing it in the liquid medium like water, ethanol, methanol etc. For larger particle size, the particles precipitate. Thus, the spectrum is mostly due to the liquid. Diffuse reflectance spectroscopy (DRS) enables us to obtain Eg of powder samples, which scatter in perfectly diffuse manner. DRS works on Kubelka and Munk model [15], in which diffuse reflectance R is related to Kubelka– Munk function F(R) by

$$F(R) = \frac{(1-R)^2}{2R} \tag{2.1}$$

where, R denotes the percentage reflectance from the sample [14,15].

A graph between $[F(R).h\nu]^2$ vs. hν (in eV) can provide the values of a sample with direct bandgap. An indirect bandgap can be obtained from a plot of $[F(R).h\nu]^{1/2}$ versus hν. Diffuse reflectance is measured by an Experimental Details 50 integrating sphere detector.

2.7 Degradation of Methylene Blue under UV Light

Methylene blue is a heterocyclic aromatic chemical compound with the molecular formula $C_{16}H_{18}ClN_3S$. It has many uses in different fields. It appears as a solid at room temperature and is odorless, and is a dark green powder that gives a blue solution when dissolved in water. We have to degrade the methylene blue. So, we require electrons so that they can convert the complex component and break it into a simple component as the electrons try to get attached to the complex structure of MB. So, first we have to prepare solution for this. We put 6mg amount of MB in 1 litter DI water than we take some amount of this sample in different-different beakers and also few ml H_2O_2 and our sample.

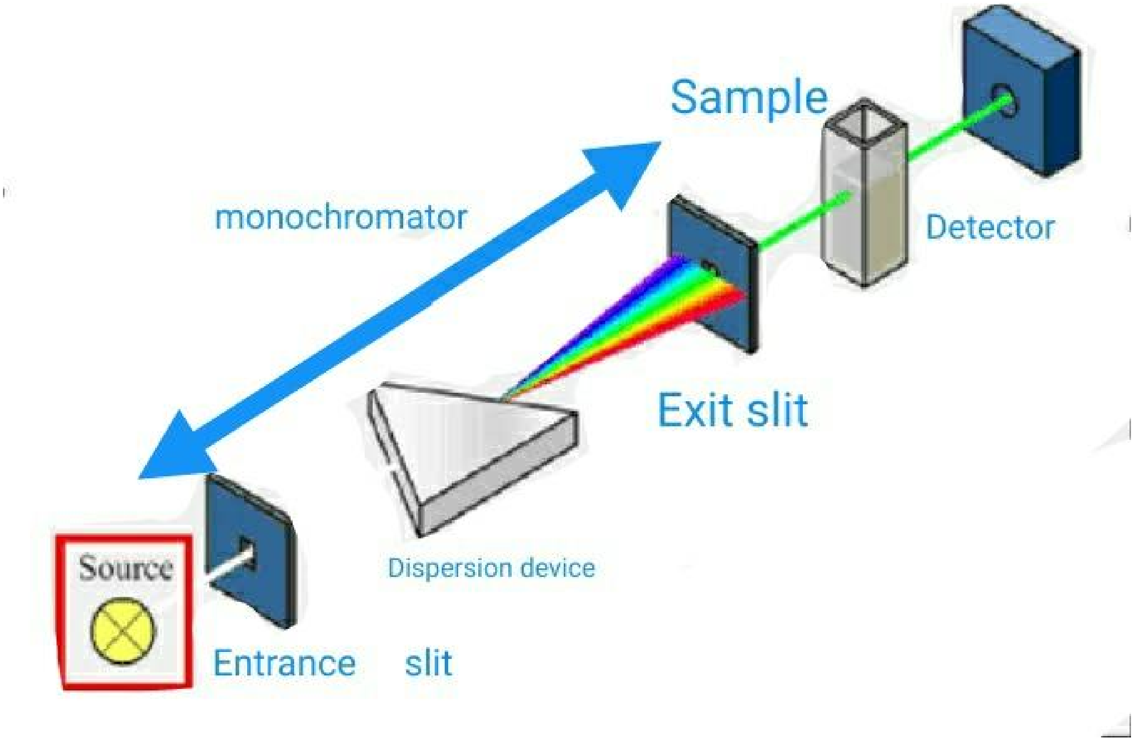

Figure 2.5: Schematic diagram for UV-Visible Spectroscopic setup

Now we put our solution under light (frequency of light depend on our sample). So, whenever we shine the light on our solutions with this energy the electron gets excited. In such manner electrons and holes pairs will generate these exited electrons attack on MB and MB start degrade. During the photodegradation process, H_2O_2 is generated. It fastens the process of photodegradation. To achieve better results, more H_2O_2 was added to the testing solution to improve MB photodegradation. During the process, H_2O_2 is decomposed, resulting in the creation of an OH radical and a hydroxyl ion:

$$H_2O_2 + e^- \rightarrow OH^0 + OH^- \tag{2.2}$$

The organic dye (MB) can be attacked and degraded by the OH radicals produced:

$$MB + OH^0 \rightarrow MB'^{\cdot} + H_2O \tag{2.3}$$

The following is a full description of the aforesaid radical production pathway. When a photon with an energy hv greater than the bandgap, Eg, i.e., hν > Eg, collides with the sample, an e-h pair is formed, which can be represented as

$$NMs + h\nu \to e^-_{CB} + h^+_{VB} \tag{2.4}$$

When adsorbed oxygen reacts with an electron, the oxidation state of oxygen is reduced from 0 to 1/2:

$$(O_2)_{ads} + e^-_{CB} \to O_2^{\cdot -} \tag{2.5}$$

The hole, on the other hand, neutralizes the OH by generating an OH^0 radical:

$$(H_2O \Leftrightarrow H + +OH^-)_{ads} + h^+_{VB} \to H^+ + OH^0 \tag{2.6}$$

The O_2^{0-} is neutralized by the remaining positive hydrogen ion :

$$O_2^{0-} + H^+ + HO_2^0 \tag{2.7}$$

As a result, transitory hydrogen peroxide and oxygen are formed:

$$2HO_2^0 \to H_2O_2 + O_2 \tag{2.8}$$

The H_2O_2 will be decomposed, resulting in the second oxygen reduction:

$$H_2O_2 + e^- \to OH^0 + OH^- \tag{2.9}$$

The OH^0 radicals that are created attack and destroy the MB dye:

$$MB + OH \to MB^{\cdot} + H_2O \tag{2.10}$$

The next paragraph goes over the deterioration process. MB +h+ MB+ degradation products are formed when the holes contribute in the degradation of the MB dye. The addition of the scavenger (H_2O2) can accelerate the degradation rate by forming OH, OH quickly. Breaking the bonds of the [C–S+=C] functional group in MB dye is the first step in MB degradation. Now we can calculate how long light we need for degradation of methylene blue. Such experiments are very useful in textile industry.

2.8 Pressure dependent I-V characteristic curve

For pressure IV we use hydraulic press The science behind hydraulics is follow Pascal's principle. Essentially, because the material in the pipe is incompressible, we know that the pressure must stay constant all the way through it, so it only depends on force and area. even when you're pushing it hard at one end or the other, such in this manner we put our sample in one end and apply pressure, and observe the I-V characteristic. Now when we put force the distance between electron clouds decreases as such electrons move faster than before. first, we start from 0 Ton of pressure, after which on increase the pressure and we observe the current increases.

This formula uses in hydraulic press

$$P = \frac{F}{A} \tag{2.11}$$

where F = force and A = area.

Chapter 3

Result & Discussion

This chapter provides characterization techniques used in present research work.

3.1 X-ray diffraction

X-ray diffraction (XRD) spectra was obtained from the Bruker D2-Phaser diffractometer. Xray source: Cu-anode (1.5406 Å). The XRD confirms the phase purity and crystal structure of Zn1- x(Al0.5Ni0.5)x (abbreviated as ZANO) at ambient temperature. The ZANO samples annealed at 450° show hexagonal wurtzite phase. The XRD data reveals multiple peaks which can confirm the structural similarities of these samples to that of ZANO. For Z(AN)S0 (x=0) peaks were observed diffraction peaks at the (100), (002), (101), (102), (110), (103), (200, (201), (004), (201), and (202) of the hexagonal.

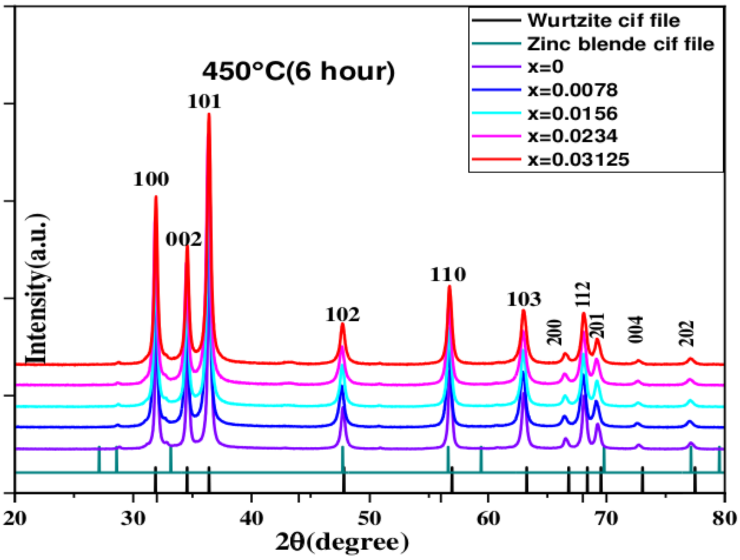

Figure 3.1: XRD pattern of Al/Ni co-doped ZnO heating at 450ºC(6 hrs)

A dominant hexagonal wurtzite ZnO structure was revealed from XRD studies as shown in Figure 3.1 - No secondary phases were found related to simple or complex oxides of Zn and Al/Ni for x < 0.03125, apart from some minor reflections of zinc blend.

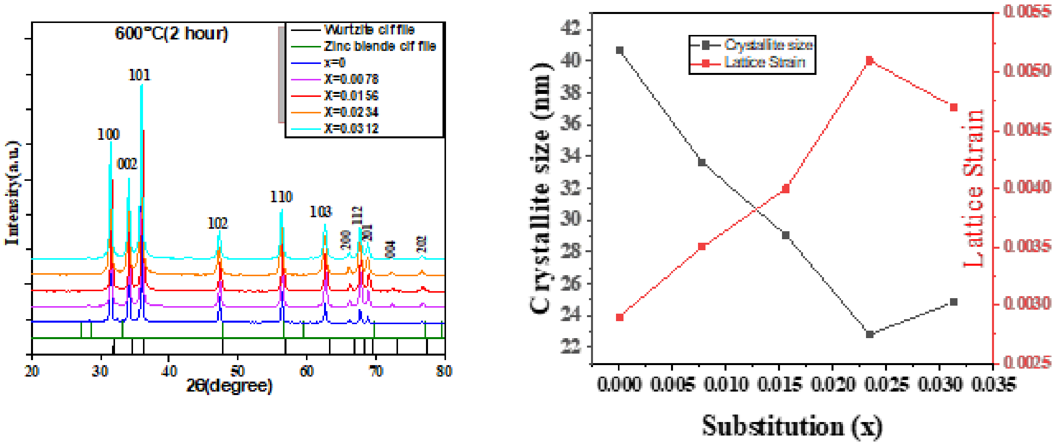

(a)

(b)

Figure 3.2: (a) XRD reveals pure single phase of samples without the presence of any impure phase. (b) Crystallite size and lattice strain from Debye-Scherer equation.

3.2 Rietveld Refinement

Refinement has been done using GSAS software with a Pseudo-Voigt profile and a 6-coefficient polynomial function background, similar to the previous refinements.

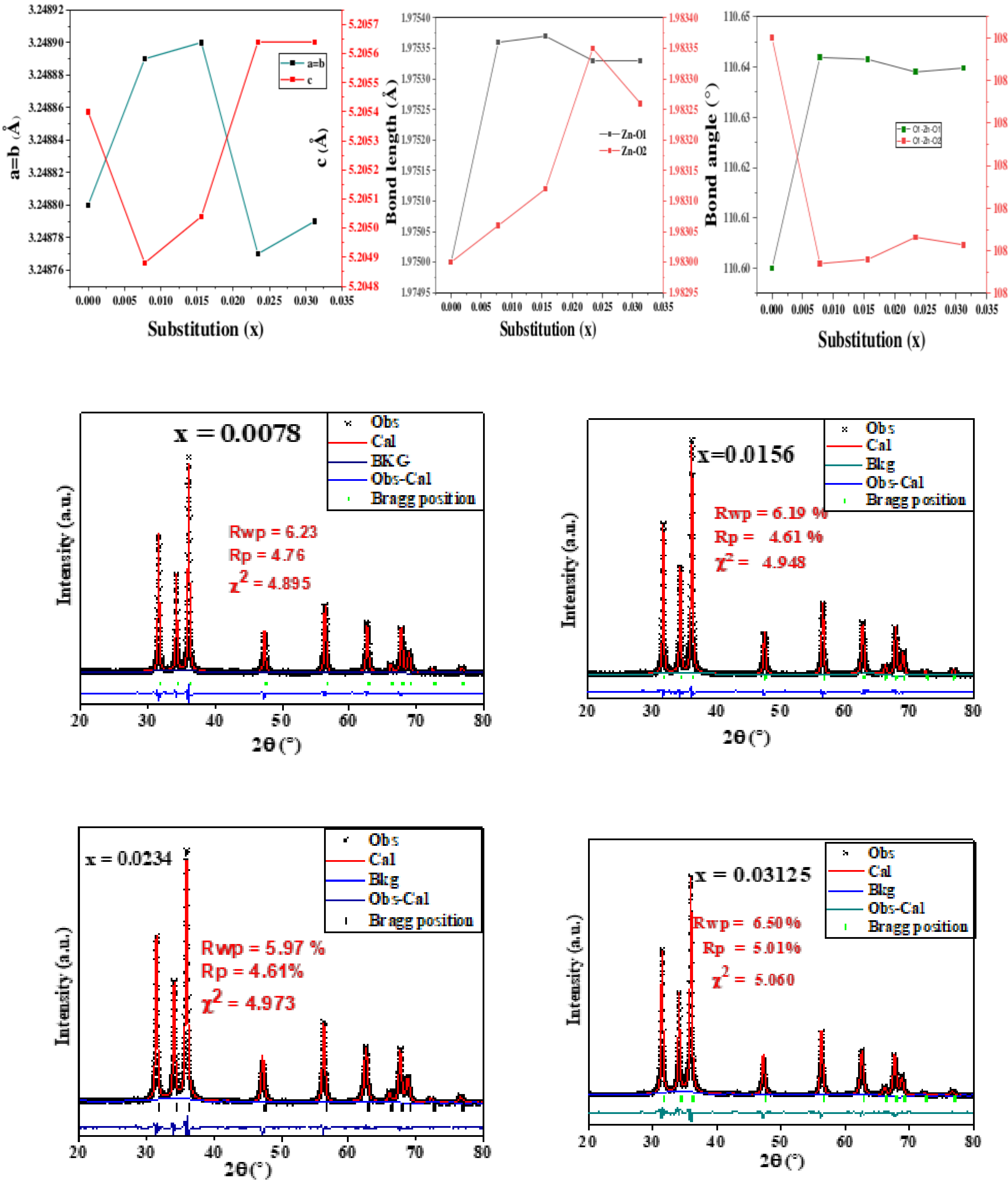

Figure 3.3: Rietveld refinement plot of the Al/Ni modified ZnO.

3.3 Raman Spectroscopy

Raman vibrational modes were studied in detail [Figure 3.5 (a)]. In hexagonal structures with C4 6v symmetry, group theory predicts eight sets of phonon normal modes, namely, 2A1+2E1+2B1+2E2. Among them, one set of A1 and E1 mode are acoustic , while the remaining six modes, namely, A1+E1+2B1+2E2 , are optical modes [16]. The A1 and E1 branches are both Structural properties of Pure and Modified ZnO Raman and infrared active, the two nonpolar E2 branches are Raman active only, and B1 branches are inactive. Raman phonon modes were also observed at $\sim$ 99 cm^{-1}, 332 cm^{-1}, 439 cm^{-1} and respectively as shown in Figure 3.5. The non- polar E2 high and E2 low modes are due to relative vibrations of oxygen and zinc sub-lattices in two different orientations along c-axis.

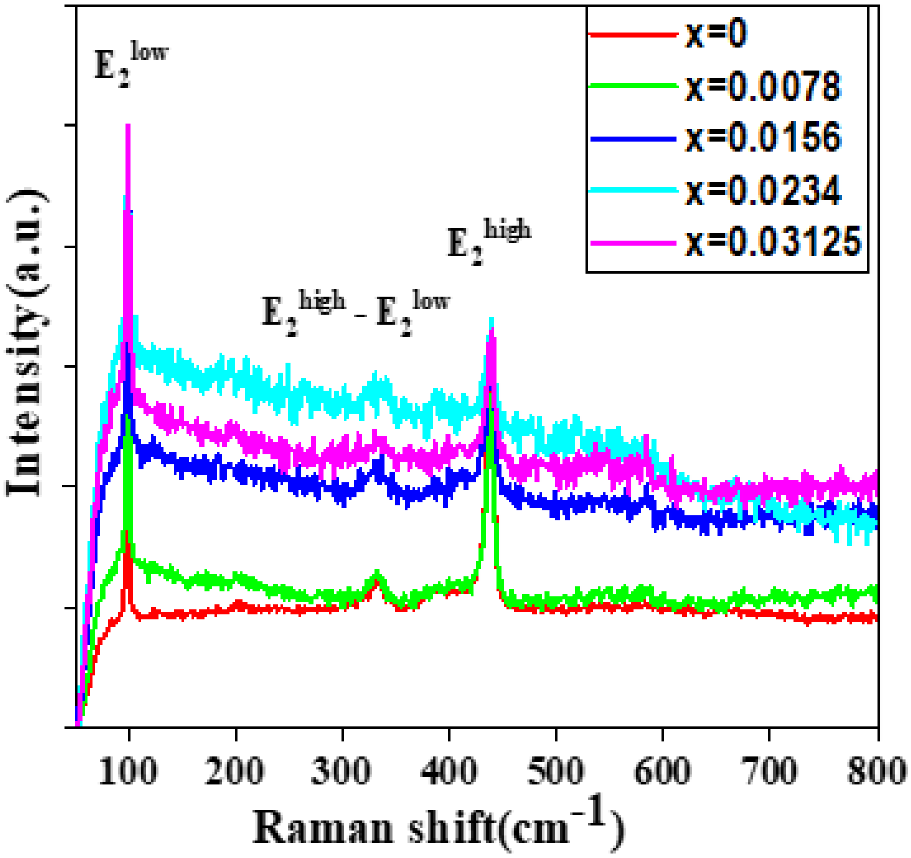

Figure 3.4: The room temperature Raman spectra of pure and Al/Ni modified ZnO annealed at 600°C

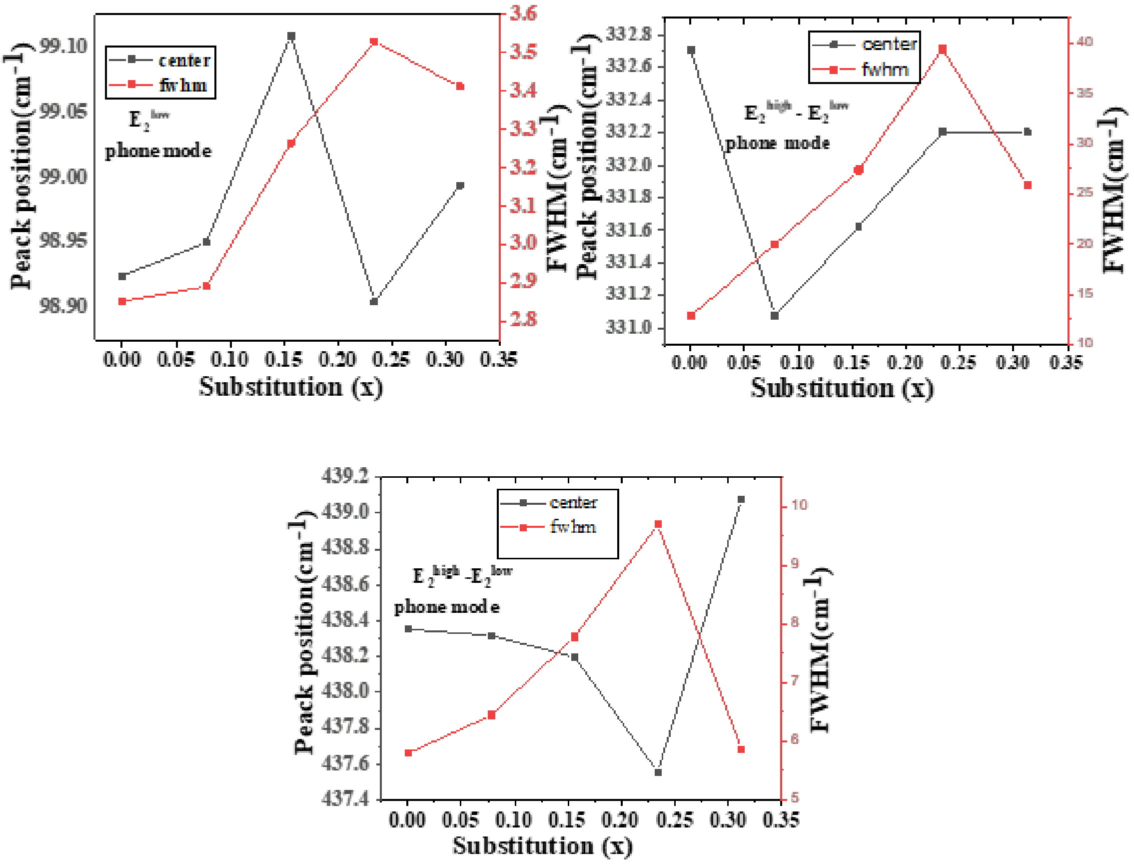

Figure 3.5: Variation in the phonon frequency and peak width with different doping concentrations Z(AN)S0, Z(AN)S1, Z(AN)S2, Z(AN)S3 & Z(AN)S4.

3.4 UV-Vis Spectroscopy

a) Band gap: When electromagnetic radiation (light) interacts with matter, various effects can be observed such as reflection, scattering, absorbance, transmittance and fluorescence/ phosphorescence. Total potential energy of a molecule can be represented as the sum of its electronic, rotational and vibrational energies. When energy of incident light is equal to the energy required to excite an electron from a lower energy level to higher level, the light is absorbed. Working Principal: Amount of light absorbed is the difference between the incident radiation (I_0) and the reflected or transmitted radiation (I). Quantitatively absorbance is described by equation: A = -log (I/I_0) where, A is absorbance, T is transmittance, I_0 and I are the intensities of incident and transmitted light respectively at a given wavelength. A UV-Vis spectrophotometer uses a tungsten-halogen or deuterium lamp as a source. A dispersion device like a monochromator is used to select the incident wavelength. A detector, which converts UV- visible light into electrical signal is the final component of the spectrophotometer. It is easy to bandgap (E_g) from absorption spectra, in case of solid films of known low thickness, due to low scattering properties. However, in colloidal samples, due to large surface area exposure scattering is enhanced. As dispersed light does not reach the detector it is counted as absorbed light. The technique (optical absorption) cannot distinguish between the two phenomena.

UV-Vis of powdered sample is carried out by dispersing it in the liquid medium like water, ethanol, methanol etc. For larger particle size, the particles precipitate. Thus, the spectrum is mostly due to the liquid. Diffuse reflectance spectroscopy (DRS) enables us to obtain Eg of powder samples, which scatter in perfectly diffuse manner. DRS works on Kubelka and Munk model [15], in which diffuse reflectance R is related to Kubelka– Munk function F(R) by

$$F(R) = \frac{(1-R)^2}{2R} \tag{3.1}$$

where, R denotes the percentage reflectance from the sample [15,26]. A graph between $[\mathrm{F(R)}.\mathrm{h}\nu]^2$ vs. $\mathrm{h}\nu$ (in eV) can provide the values of a sample with direct bandgap. An indirect bandgap can be obtained from a plot of $[\mathrm{F(R)}.\mathrm{h}\nu\ ]^{1/2}$ versus $\mathrm{h}\nu$. Diffuse reflectance is measured by an integrating sphere detector UV-Vis spectrometer.

Eg can be observed in 450° ZANS1 (∼3.207 eV) and ZANS2 (∼3.271 eV) ZNS0 (∼3.278 eV). The Eg value of ZANS3 (∼3.209 eV) ZANS4 (∼3.258 eV) and S5 (∼3.396 eV). This result show very fluctuating result for more precisely further annealing at 600° here we can observe that bandgap cross ponding Z(AN)S0 (∼3.27391 eV) and Z(AN)S1 (∼3.26811eV) Z(AN)S2(∼3.26345eV), Z(AN)S3(∼3.25763eV) and ZANS (∼3.258966eV).

b) Urbach Energy: Appearance of Urbach tail is due to structural disorder and strain, caused by structural defects due to vacancies, dopants. ZnO lattice, naturally, have lots of vacancies and defects. These may contribute to structural disorders. These disordered states can be observed as band tails in the UV-vis absorption edge for energy, $\mathrm{h}\nu <$ Eg the Urbach energy, Eu, of the system can be used to estimate such disorder. In comparison to Z(AN)S0 83.271 meV), the Eu decreases for Z(AN)S1 (91.0166 meV) and Z(AN)S2 (100.1307 meV), then increases for Z(AN)S3 (105.28532 meV), Z(AN)S (109.5 meV) here we can see urbach energy increasing so that's mean distortion increase inset of figure 3.8).

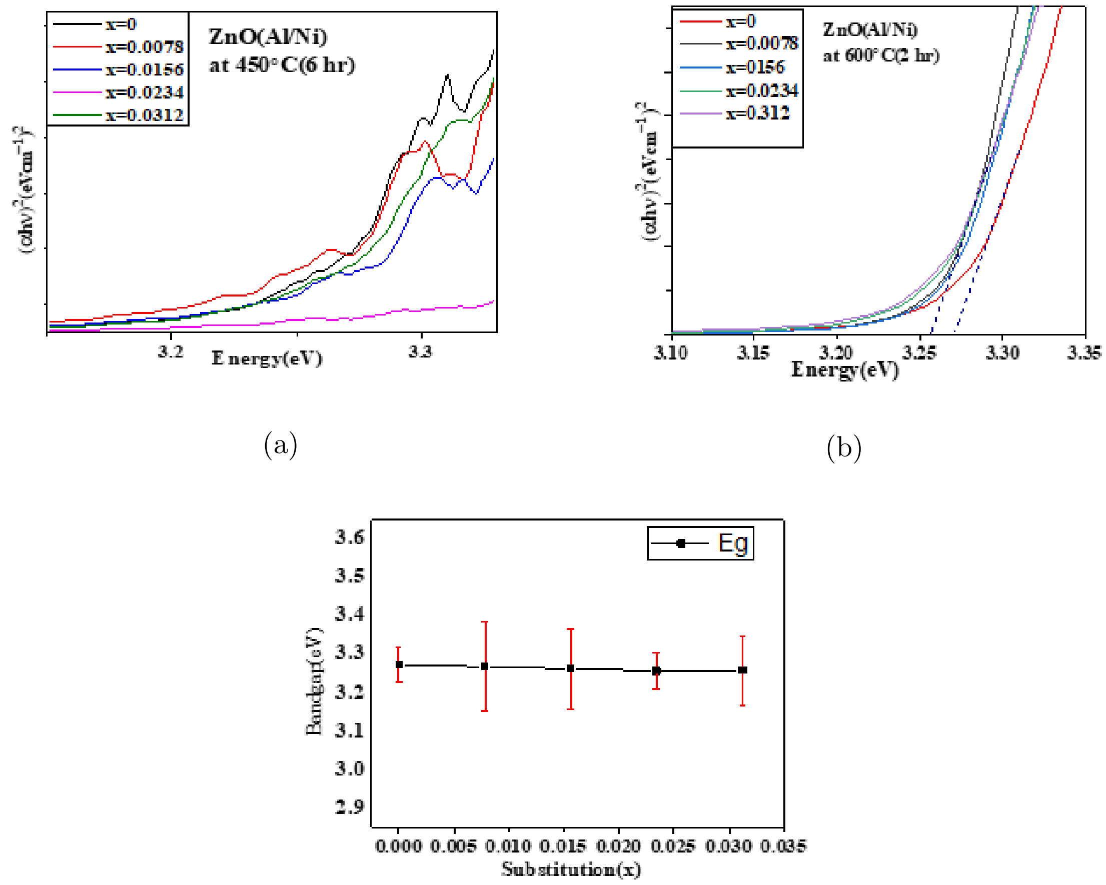

(a)

(b)

(c)

Figure 3.6: Tauc plot for band gap from UV-Vis spectroscopy. (a)ZALO at 450° (6 hrs), (b) a)ZALO at 600° (2 hrs), (c) variation in band gap energy for ZALO at 600° (2 hrs) .

Urbach energy has been calculated using the empirical Urbach relation [27]:

$$\alpha = \alpha_0 \, exp \, (\frac{h\nu}{E_U})(h\nu \; E_U) \tag{3.2}$$

where, α_0 is a constant, E_U is the Urbach energy. Slope of a ln (α) versus hν plot provides estimation of E_U (Figure 3.7)

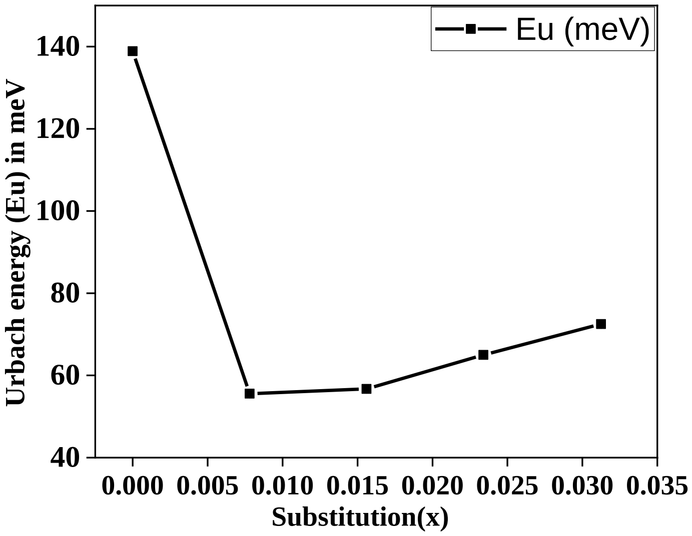

1

Figure 3.7: Variation in Urbach energy

3.5 Pressure-I-V characterization

The pressure-dependent I-V characteristics of all the prepared samples were investigated. The results were repeatable, and the experiment was repeated on the same sample numerous times before being repeated on different specimens of the same composition. For the Z(AN)S0 sample, the differences are minor. The current rose continuously with applied pressure from Z(AN)S0 to Z(AN)S4 at 1.0 V applied voltage. It's also worth noting that the current rises steadily from Z(AN)S0 through Z(AN)S1, Z(AN)S2, and Z(AN)S3, before rapidly increasing for Z(AN)S3. For Z(AN)S2, and Z(AN)S4, the modifications are insignificant. However, the effects of adding extra Al/Ni appear to be dramatic. As a result, it becomes clear that greater quantities of Al/Ni ions play a key role in improving charge transfer in the presence of pressure, which could be attributable to contributions from modified Zn^{2+} ion electron clouds due to Al^{3+} ion doping and therefore the presence of Vo's. The quantity of current generated owing to pressure in the Z(AN)S1 sample does not so much dependency on pressure but further when we increasing doping the current rapidly increasing. Z(AN)S4 samples is less than in the Z(AN)S3 sample, may be indicating that as Al^{3+} incorporation increases, conductivity decreases may be due to an increase in Oi. As a result, it is clear that increasing Vos in the lattice improves conductivity.

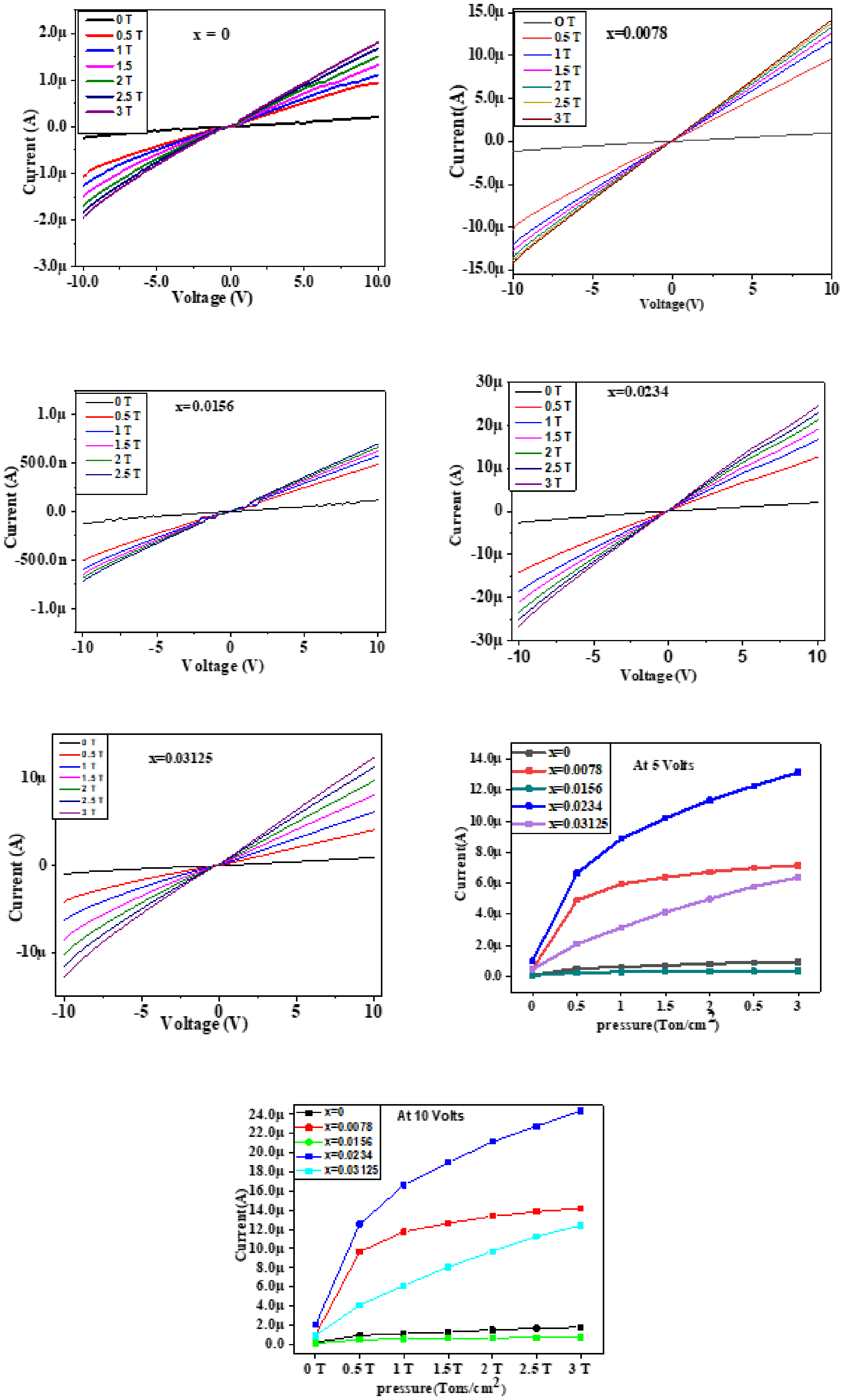

Figure 3.8: Pressure dependent current vs voltage plots (I-V characteristics) for $Zn_{1-x}(Al_{0.5}Ni_{0.5})_x$, $0 \leq x \leq 0.03125$.

3.6 Degradation of Methylene blue under UV light

Degradation of MB is successfully done by using pure and modified ZnO. Here we are doing temperature dependent degradation so first we start experiment for temperature optimization so here we can in Figure 3.9(a) we shine the light for same time interwall with different temperature. we can observe from figure 3.9 (b) that at 53°C temperature degradation of MB is highest percentage. In figure 3.9(c) we can see sample ZANS3 have highest capability of degrading MB. Now we vary the catalyst. In figure 3.9(d) 30mg amount of sample degrade maximum percentage. there are many more factor which affects reaction rate like- environment temperature, PH medium and extra addition of radicals. Here we using H_2O_2 as radical. So, 1.49 molar of H_2O_2 have maximum percentage of degradation. In Figure 3.10, we Observe that modified ZnO can degrade MB in just 30 minutes. So, we conclude that we can modify the photo catalyst properties by modifying ZnO.

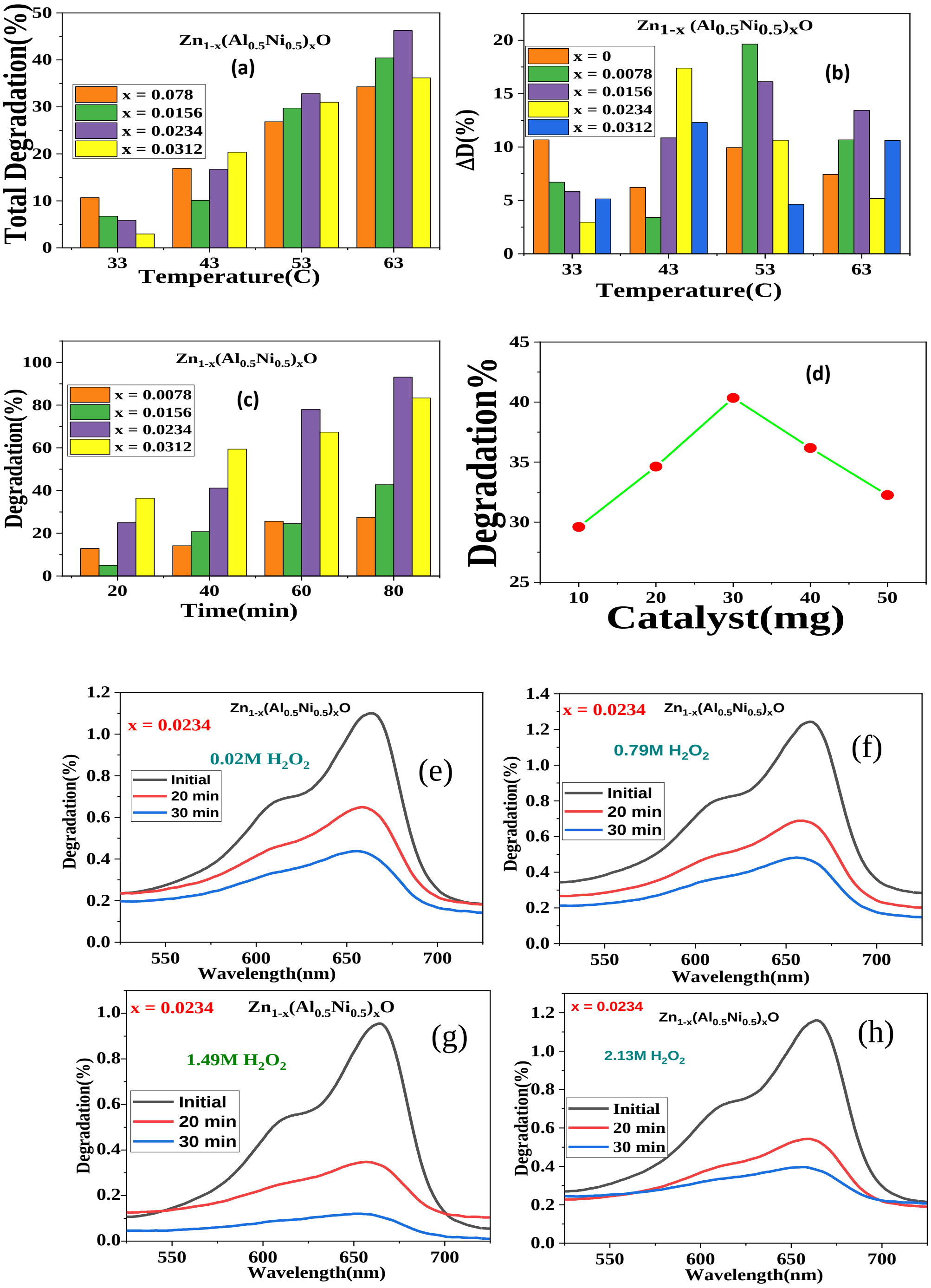

Figure 3.9: (a) & (b) shows degradation vs temperature of MB; (c) show temperature vs time of MB; (d) shows degradation variation with catalyst of MB; (e, f, g, h) shows degradation vs wavelength.

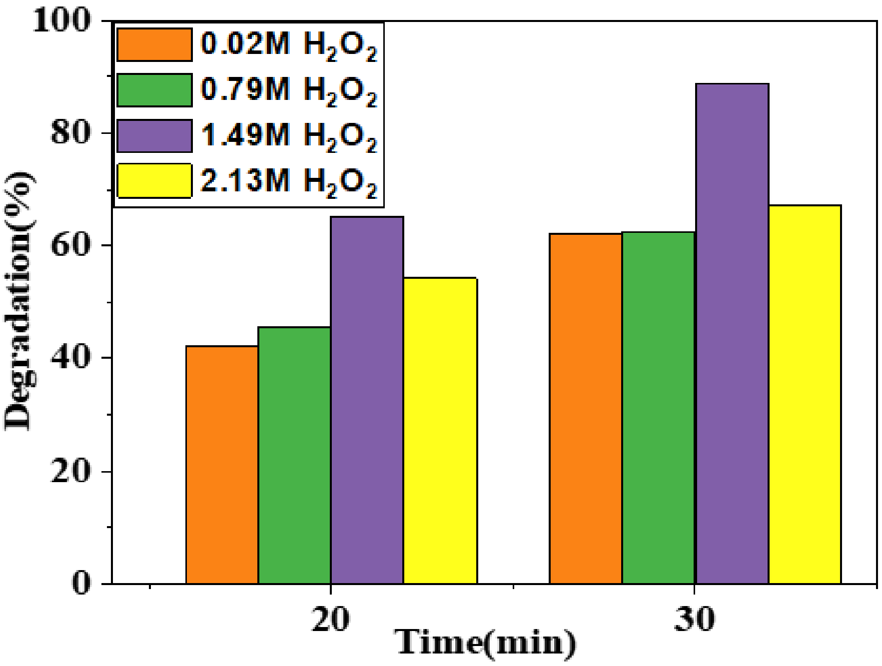

Figure 3.10: Degradation versus time plot for different molarity of H_2O_2.

Summary

ZnO nanopowder prepared using very simple and useful sol gel method gave quite positive results with pure ZnO phase formed at 450 °C. It can also be seen that just by varying some of the precursor elements used, Sol- gel prepared $\mathrm{Zn_{1-x}(Al_{0.5}Ni_{0.5})_xO}$ nanoparticles revealed a generally crystalizes in three forms: Hexagonal Wurtzite, Cubic Zinc Blende and Rock salt structure. group of P63mc the host cation being Zn^{2+}, the Al^{3+} doped system is an oxygen rich system due to the extra positive charge of Al^{3+} as compared to ZnO. In XRD plots the highest intensity peak shifting so according to bragg's law we can observed that d spacing varies in Modified sample so various property should be modified.
Rietveld refinement show goodness of fit from that we can see bond length and bond angle not change much.
UV-Vis plots show that band gap is reduced respect to pure so may be some defects state is generating between V.B. and C.B. but there is very less change in band gap. In other manner Urbach energy shows distortion in lattice. In urbech energy plots we can see urbech energy reduce in modified ZnO respect to pure one. So, distortion in lattice may decrease.
From pressure dependent I-V characterization we can say when doping precents increase conductive properties also increases with pressure. Dye degradation - The photocatalytic degradation of toxic methylene blue (MB) dye could be enhanced from 0.56%/min for the pure ZnO to 1.29%/min for $x_0 \leq \mathrm{x} \leq 3.125\%$ Al/Ni doped ZnO. We degrade MB using these sample so reaction rate of modified sample is far more than pure sample so by modifying ZnO we can improve their photocatalytic properties.
So, all we can conclude that by modifying ZnO we can modify there optoelectronic and photocatalytic properties. Still FESEM and Photoluminescence Spectroscopy needs to do for recognize the defect states.

References

1. V.A. Coleman, C. Jagadish, Chapter 1 - Basic Properties and Applications of ZnO, in: Zinc Oxide Bulk Thin Films Nanostructures, Elsevier Science Ltd, Oxford, 2006: pp. 1–20. doi:10.1016/B978-008044722- 3/50001-4.

2. Z.L. Wang, Zinc oxide nanostructures: growth, properties and applications, J. Phys. Condens. Matter. 16 (2004) R829. doi:10.1088/0953-8984/16/25/R01.

3. B.K. Meyer, H. Alves, D.M. Hofmann, W. Kriegseis, D. Forster, F. Bertram, J. Christen, A. Hoffmann, M. Straßburg, M. Dworzak, U. Haboeck, A.V. Rodina, Bound exciton and donor–acceptor pair References 150 recombinations in ZnO, Phys. Status Solidi B. 241 (2004) 231–260. doi:10.1002/pssb.200301962.

4. A. Mang, K. Reimann, S. Rübenacke, Band gaps, crystal-field splitting, spin-orbit coupling, and exciton binding energies in ZnO under hydrostatic pressure, Solid State Commun. 94 (1995) 251–254. doi:10.1016/0038-1098(95)00054-2.

5. D.C. Look, Recent advances in ZnO materials and devices, Mater. Sci. Eng. B. 80 (2001) 383–387. doi:10.1016/S0921-5107(00)00604- 8.

6. Ü. Özgür, Y.I. Alivov, C. Liu, A. Teke, M.A. Reshchikov, S. Doğan, V. Avrutin, S.-J. Cho, H. Morkoç, A comprehensive review of ZnO materials and devices, J. Appl. Phys. 98 (2005) 041301. doi:10.1063/1.1992666.

7. N.H. Nickel, E. Terukov, Zinc Oxide - A Material for Micro- and Optoelectronic Applications: Proceedings of the NATO Advanced Research Workshop on Zinc Oxide as a Material for Micro- and Optoelectronic Applications, held in St. Petersburg, Russia, from 23 to 25 June 2004, Springer Science & Business Media, 2006.

8. F. Tuomisto, K. Saarinen, D.C. Look, G.C. Farlow, Introduction and recovery of point defects in electron- irradiated ZnO, Phys. Rev. B. 72 (2005) 085206. doi:10.1103/PhysRevB.72.085206.

9. D.C. Look, J.W. Hemsky, J.R. Sizelove, Residual Native Shallow Donor in ZnO, Phys. Rev. Lett. 82 (1999) 2552–2555. doi:10.1103/PhysRevLett.82.2552.
10. S.R. Shinde, S.B. Ogale, J.S. Higgins, H. Zheng, A.J. Millis, V.N. Kulkarni, R. Ramesh, R.L. Greene, T. Venkatesan, Co-occurrence of Superparamagnetism and Anomalous Hall Effect in Highly Reduced Cobalt- Doped Rutile $TiO_{2-\delta}$ Films, Phys. Rev. Lett. 92 (2004) 166601. doi:10.1103/PhysRevLett.92.166601.
11. M.A. García, M.L. Ruiz-González, A. Quesada, J.L. Costa-Krämer, References 151 J.F. Fernández, S.J. Khatib, A. Wennberg, A.C. Caballero, M.S. Martín-González, M. Villegas, F. Briones, J.M. González-Calbet, A. Hernando, Interface Double-Exchange Ferromagnetism in the MnZn-O System: New Class of Biphase Magnetism, Phys. Rev. Lett. 94 (2005) 217206. doi:10.1103/PhysRevLett.94.217206.
12. S.D. Yoon, Y. Chen, A. Yang, T.L. Goodrich, X. Zuo, D.A. Arena, K. Ziemer, Carmine Vittoria, V.G. Harris, Oxygen-defect-induced magnetism to 880 K in semiconducting anatase TiO 2-δ films, J. Phys. Condens. Matter. 18 (2006) L355. doi:10.1088/0953- 8984/18/27/L01.
13. M. Havrdova, K. Polakova, J. Skopalik, M. Vujtek, A. Mokdad, M. Homolkova, J. Tucek, J. Nebesarova, R. Zboril, Field emission scanning electron microscopy (FE-SEM) as an approach for nanoparticle detection inside cells, Micron. 67 (2014) 149–154. doi:10.1016/j.micron.2014.08.001.
14. Raman Spectroscopy - Theory and Practice || H.A. Szymanski || Springer, n.d. //www.springer.com/gp/book/9781468430264 (accessed January 7, 2018).
15. A. Escobedo Morales, E. Sánchez Mora, U. Pal, Use of diffuse reflectance spectroscopy for optical characterization of un-supported nanostructures, Rev. Mex. Fis. Suppl. 53 (2007) 18–22 .
16. H. Morkoç, Ü. Özgür, General Properties of ZnO, in: Zinc Oxide, References 165 Wiley-VCH Verlag GmbH & Co. KGaA, 2009: pp. 1–76. doi:10.1002/9783527623945.ch1.
17. M. Bououdina, S. Azzaza, R. Ghomri, M.N. Shaikh, J.H. Dai, Y. Song, W. Song, W. Cai, M. Ghers, Structural and magnetic properties and DFT analysis of ZnO:(Al,Er) nanoparticles, RSC Adv. 7 (2017) 32931– 32941. doi:10.1039/C7RA01015J.
18. S. Singh, M.S.R. Rao, Optical and electrical resistivity studies of isovalent and aliovalent 3*d* transition metal ion doped ZnO, Phys. Rev. B. 80 (2009) 045210. doi:10.1103/PhysRevB.80.045210.

19. R.D. Shannon, Revised effective ionic radii and systematic studies of interatomic distances in halides and chalcogenides, Acta Crystallogr. A. 32 (1976) 751–767. doi:10.1107/S0567739476001551.

20. N. Rashidi, V.L. Kuznetsov, J.R. Dilworth, M. Pepper, P.J. Dobson, P.P. Edwards, Highly conducting and optically transparent Si-doped ZnO thin films prepared by spray pyrolysis, J. Mater. Chem. C. 1 (2013) 6960–6969. doi:10.1039/C3TC31129E.

21. A.K. Das, P. Misra, L.M. Kukreja, Effect of Si doping on electrical and optical properties of ZnO thin films grown by sequential pulsed laser deposition, J. Phys. Appl. Phys. 42 (2009) 165405. doi:10.1088/0022- 3727/42/16/165405.

22. R. Chowdhury, S. Adhikari, P. Rees, Optical properties of silicon doped ZnO, Phys. B Condens. Matter. 405 (2010) 4763–4767. doi:10.1016/j.physb.2010.08.072.

23. I. Sorar, D. Saygin-Hinczewski, M. Hinczewski, F.Z. Tepehan, Optical and structural properties of Si- doped ZnO thn films, Appl. Surf. Sci. 257 (2011) 7343–7349. doi:10.1016/j.apsusc.2011.03.142.

24. M.H. Farooq, H.-L. Yang, X.-G. Xu, C.-J. Ran, J. Miao, M.Y. Rafique, L.-Q. Pan, Y. Jiang, Room temperature ferromagnetism of Si-doped ZnO thin films prepared by sol–gel method, Rare Met. 32 (2013) 165–168. doi:10.1007/s12598-013-0048-7.

25. Wiley: Zinc Oxide: Fundamentals, Materials and Device Technology - Hadis Morkoc, Ümit Ozgur, (n.d.). http://www.wiley.com/WileyCDA/WileyTitle/productCd3527408134.ht (accessed January 15, 2017).

26. H. Deng, J.M. Hossenlopp, Combined X-ray diffraction and diffuse reflectance analysis of nanocrystalline mixed Sn(II) and Sn(IV) oxide powders, J. Phys. Chem. B. 109 (2005) 66–73. doi:10.1021/jp047812s

27. S.J. Ikhmayies, R.N. Ahmad-Bitar, A study of the optical bandgap energy and Urbach tail of spray- deposited CdS:In thin films, J. Mater. Res. Technol. 2 (2013) 221–227. doi:10.1016/j.jmrt.2013.02.012

28. Tulika Srivastava, E. G. Rini, Ashutosh Joshi, Parasharam Shirage, and Somaditya Sen, “Structural Distortion and Bandgap Increment in Nanocrystalline Wurtzite Si Substituted ZnO” Journal of anoscience and Nanotechnology,16, 1–4, 2016.

29. Tulika Srivastava, Sunil Kumar, Parasharam Shirage, Somaditya Sen, “Reduction of O2– related defect states related to increased bandgap in Si + substituted ZnO” Scripta Materialia, 124, 11–14, 2016.

30. Tulika Srivastava, Gaurav Bajpai, Nidhi Tiwari, Dibyendu Bhattacharya, S. N. Jha, Sunil Kumar, Sajal Biring, and Somaditya Sen, “Opto-electronic properties of Zn(1-x) VxO: Green emission enhancement due to V + state” Journal of Applied Physics 122, 025106, 2017.

31. Tulika Srivastava, Aswin Sadanandan, Gaurav Bajpai, Saurabh Tiwari, Ruhul Amin, Mohd. Nasir, Sunil Kumar, Parasharam M. Shirage, Sajal Biring, Somaditya Sen, “Zn1-xSixO: Improved optical transmission and electrical conductivity” Ceramics International, 3, 5668–5673, 2017.

32. Tulika Srivastava, Gaurav Bajpai, Gyanendra Rathore, Sajal Biring, Somaditya Sen, “Vanadium substitution: a simple and efficient way to improve UV sensing in ZnO” Journal of Applied Physics, 123, 161 07, 2018. VI. Tulika Srivastava, Gaurav Bajpai, Shun Wei Liu, Sajal Biring, Somaditya Sen, “Zn1-xSixO: Reduced photosensitivity, improved stability and enhanced conductivity” Scripta Materialia, 150, 42-44, 2018.